Iron Mining Waste as sustainable material for producing bricks: microstructure, mechanical and thermal properties.

Hadjer Bouzeriba ¹, Nedjima Bouzidi ^{1*}, Abdelaziz Idres ², Imen Laala ¹, Farid Ait Merzeg ^{1,3}

¹ University of Bejaia, Faculty of Technology, Laboratory of Materials Technology and Process Engineering

(LTMGP) 06000 Bejaia, Algeria;

²University of Badji Mokhtar, Faculty of Earth Sciences, Laboratory of Mineral Resources Valorization and

Environment (LAVAMINE) Annaba, Algeria;

³Technical Platform for Physico-chemical Analyzes (PTAPC-Bejaia), Targa Ouzemmour, 06000 Bejaia, Algeria

(*) corresponding author: nedjima.bouzidi@univ-bejaia.dz

Submitted: 13 March 2025. Revised 6 October 2025. Associate Editor: Michele Dondi

Abstract

Iron Mining Waste are produced from iron ore mining operations of El Ouenza mine (North-East Algeria) are rejected and are not currently recycled to preserve the environment. The current study aims at developing sustainable clay-bricks by mixing clay with different proportions of Iron Mining Waste (ranging from 10 to 50 wt %) and fired at 850 and 950 °C. Addition of 30 wt% of the Iron Mining Waste had a positive effect on physical and mechanical properties of the fired clay bricks. Linear shrinkage, water absorption and porosity were reduced, while compressive and flexural strengths increased. Furthermore, up to 30 wt% of Iron Mining Waste addition in the mixtures improved compressive and flexural strength to 59.17 MPa and 10.06 MPa respectively, when the bricks were fired at 950 °C. According to their thermal conductivity, the bricks with 10-50 wt% of Iron Mining Waste are considered as thermal insulators with thermal conductivity ranging from 0.45 to 0.56 Wm⁻¹K⁻¹. Adding 30 wt% of Iron Mining Waste can produce eco-friendly bricks since it could cause economic and environmental benefits with high mechanical and thermal performances.

Keywords: El-Ouenza Mine; Iron Mining Waste; clay bricks; Mechanical properties; Thermal conductivity; Environment.

1

INTRODUCTION

The need to seek and build new infrastructures, has contributed to the growing increase in building materials, due to rapid urban expansion, industrialization and development of countries (Idrees et al., 2023). The manufacturing of construction materials, including cement, concrete, bricks, and ceramic tiles, is a pivotal sector that is significant for national economies (Xin et al., 2023). Over the last few decades, bricks have become one of the most popular building materials used throughout the world (Weishi et al., 2018). Generally, two main types of bricks are manufactured commercially, one based on cement and the other on clay (Ozturk et al., 2019).

Clay masonry brick is among the oldest and most widely used construction techniques, with a rich historical background (Bai et al., 2023), as the first clay brick was used as early as 4500 BC (Shi et al., 2023; Rashid et al., 2023). Bricks are among the most commonly utilized construction materials due to their utility, superior strength, reduced manufacturing costs, enhanced fire resistance, durability against chemical exposure, corrosion and exposure to freeze-thaw cycles, longevity, and ease of production (Dabaieh et al., 2020; Hafez et al., 2022). The manufacturing process for clay bricks involves extracting, crushing and mixing the raw materials and molding them by pressing or extrusion. Once the bricks have taken shape, they are dried and fired in a kiln at high temperature (at ~ 1200 °C) (Xin et al., 2023). However, during firing the combination of SiO₂ and Al₂O₃ with other components of the clay contributes to the establishment of a connection that imparts the bricks their distinctive strength and durability (Phonphuak et al., 2016). The manufacture of fired bricks is linked to considerable environmental consequences, including the exhaustion of raw materials and the release of greenhouse gases, environmental degradation and ecosystem disruption (Rashid et al., 2020; Raut et al., 2020).

In this respect, several countries around the world have limited the use of raw materials such as clay (Sutcu et al., 2016). In this context, the construction sector has developed most of the concepts of sustainability in order to minimize the depletion of raw materials (Božič et al., 2023). Utilizing several waste materials in the manufacturing of fired bricks can effectively mitigate substantial quantities of waste generated by various industrial processes and partially or totally replacing clay (Slimanou et al.,2020; Dos Reis et al., 2020). Several synthesis studies have been conducted to examine the application of diverse waste materials in brick manufacture, including fly ash and bottom ash (Sutcu et al., 2019), dredging sediments

(Slimanou et al., 2020; Thomas et al., 2021), glass waste (Phonphuak et al., 2019), sewage sludge (Detho et al., 2024), diatomite from the vegetable oil refining and brewing industries (Galán-Arboledas et al., 2017), agricultural biomass wastes (Maafa et al., 2023), marble waste (Sutcu et al., 2015), iron ore residues (Li et al., 2019; Vilela., 2020; Silva Ramos et al., 2024) and phosphate sludge (Ettoumi et al., 2021).

Iron Mining Waste (IMW) refers to the solid byproducts produced during the mining or processing of iron ore (Thejas et al., 2022). The chemical composition of iron ore waste mainly composts of SiO₂, Al₂O₃, Fe₂O₃ and CaO, similar to that of natural clay, and may serve as raw materials for the production of construction materials (Yang et al., 2014; Weishi et al., 2018). The integration of iron ore waste in brick manufacturing is considered as non-hazardous and poses no environmental risk. Their use has improved brick properties such as density, porosity, water absorption, mechanical strengths and reduced linear shrinkage (Thejas et al., 2022).

In Algeria, mining of El Ouenza iron ore makes a significant contribution to the country's economy, with an average iron content of 50 wt%. It is the main supplier of iron ore of El Hadjar steel complex for the production of steel and other metals (Boutarfa et al., 2023). During iron ore beneficiation, El Ouenza mine ((Tebessa, Algeria) generates large quantities of wastes estimated for 11 Mt of mine rejects compared to 36Mt of iron ore extracted (Mine documentation, 2024). Recent studies investigated the valorization of iron ore wastes produced by several separation techniques aiming at elimination of hazardous elements and enrichment of iron. Separation techniques included magnetic separation (Bouzeriba et al., 2025), radiometric separation (Baala et al., 2018) and electrostatic separation (Idres et al., 2016). As of today, recycling of these wastes (waste rocks, IMW, limestone and low-grade iron ore) in the field of sustainable materials has not been carried out in Algeria. These wastes are stocked in piles or are tailings near the mining site; this could have negative impacts on human health, environmental destruction, water pollution, social problems and air pollution (Zhang et al., 2021).

In this study, for the first time, the applicability of one of the wastes, IMW from iron ore mining operations at El Ouenza mine, was investigated for the production of clay bricks. The aim of this study is to evaluate the physical, mechanical, structural, thermal and environmental properties of fired bricks incorporating IMW as the main additive. The bricks obtained by mixing clay and different amount of IMW (0, 10, 20, 30, 40 and 50 wt %) were dried and fired at 850 and 950 °C. Effects on physical properties including density, porosity

water absorption and shrinkage on mechanical strengths and thermal conductivity were also explored.

MATERIALS AND METHODS

Materials

Approximately 20 kg of clay was collected from the Bouteldja region (19 km from El Taref province) in North-East Algeria for use in brick making. In addition, 25 kg of IMW from iron ore mining operations was taken from the stock of landfill sites on level 845 near the mining site. Before analysis, the raw materials were dried at 105 °C for 24 h, homogenized, crushed, ground and sieved to 125 μm. The bricks made from the mixing of IMW and clay was produced using the laboratory's pilot procedures and equipment. The mixtures were prepared by adding 0, 10, 20, 30, 40 and 50 wt % of IMW and were labeled MB0, MB10, MB20, MB30, MB40 and MB50 respectively. Clay bricks without IMW were produced as a reference specimen (MB0) (Fig. 1).

Methods

The plasticity index of the raw materials was assessed with the Atterberg limit test in accordance with the ASTM D 4318-17e1 standard (Ravisankar et al., 2010). Samples for liquid limit (LL) and plastic limit (PL) testing were sieved at 400 μ m. Chemical composition of the IMW and the clay was determined by X-ray Fluorescence (XRF) spectroscopy with a S8 tiger Bruker XRF spectrometer using the pressed pellet method. The mineralogical composition of raw materials and fired bricks was identified with X-ray Diffraction (XRD) using a PANalytical advanced diffractometer (EMPYREAN) with a Cu anticathode (λ = 1.54186 Å) in the scanning range 8- 55 °2 θ , with step size of 0.017°. The X'Pert High Score Plus software was used to identify the mineral species. The mineralogical composition (wt%) of the two raw materials were estimated by the mass fraction of the identified phases using the Reference Intensity Ratio (RIR) values from the database selected for the qualitative identification (Wolff & Visser, 1964; Hubbard & Snyder, 1988). Thermal analysis (TGA/DSC) of raw materials was carried out with a Perkin Elmer analyzer (STA8000) operating under air flow, at a heating rate of 10 °C/min from ambient temperature to 1100 °C.

The mixtures were mechanically mixed in a planetary mixer, for 5 min to obtain a homogeneous mixture. The samples were then mixed progressively with ~ 15 to 20% by weight water (Idrees et al., 2023), to obtain adequate plasticity without defects such as cracks, and to ensure complete homogenization. The semi-dry mixes were pressed in a $(4\times4\times16 \text{ cm}^3)$

mould under a pressure of 20 MPa using a hydraulic press (Yang et al., 2014). The test mould was sprayed with oil to prevent any effect of the inner mould wall on the sample (Ravisankar et al., 2010). The formed samples remained at room temperature for 24 hours post-extraction from the molds, followed by drying at 105 °C for 24 hours to yield dry bricks (Lamani et al., 2016). The dried bricks were fired in an electric muffle kiln (Nabertherm) at a heating rate of 3 °C/min to target temperatures of 850 and 950 °C, maintained for 1 hour at the specified firing temperature to achieve strength. Subsequent to firing, the bricks were cooled to ambient temperature through natural air convection within the kiln.

The physical and mechanical properties of the bricks were assessed in relation to ASTM construction standards for bricks. Total Linear shrinkage was evaluated by directly measuring the sample pre- and post-curing length, employing a vernier caliper to ascertain the length of the samples before and after firing, in compliance with ASTM C531. The apparent density, porosity, and water absorption of the fired bricks were assessed using ASTM C20 (Lang et al., 2020). The compressive strength test was conducted on all brick samples following ASTM C67 (Ahmad et al., 2017), utilizing a hydraulic compression machine (BeraTest) with a maximum load capacity of 2000 kN, at a loading rate of 0.5 kN/s. The load was applied incessantly to the samples until failure occurred. The flexural strength of various fired bricks was assessed per ASTM C67 (Ahmad et al., 2017) using a three-point bending method with a 10 mm span between the support knife edges. This was conducted with a BeraTest mechanical testing machine, which has a maximum capacity of 150 kN, at a loading rate of 0.5 kN/s until failure occurred. Fourier Transform Infrared (FTIR) analysis was performed with KBr pellet technique by thorough mixing 2 mg of the materials with 100 mg of KBr via grinding in an agate mortar and placing the mixtures in a press to obtain discs under high pressure using an appropriate dye. The FTIR spectra for all materials were obtained within the range of 4000-400 cm⁻¹ with a Thermo Scientific iS5 series FTIR spectrometer. Scanning electron microscopy (SEM) was employed to examine the microstructures of fired bricks, utilizing an FEI QUANTA 250 model electron microscope operating at 25 kV, equipped with an energy dispersive spectroscopy analyzer (EDS).

The thermal conductivity of the bricks was determined with a CT-meter according to the NF EN ISO 8894-1 2010 standard (Gueffaf et al., 2020). The heating duration for each

measurement was ~ 300 seconds. Each result signifies the mean of three measurements conducted on each sample.

Environmental assessment involved evaluating the mobility of contaminants using the Toxicity Characteristic Leaching Procedure (TCLP). The brick samples were pulverized and sieved through a 9.5 mm sieve to acquire a representative sample for testing. Subsequently, the extraction solution was defined by examining the pH of the sample at an 1:20 solid/liquid ratio. The extraction fluid for 1L comprised 5.7 ml of acetic acid and water, with the pH having been previously established. The tested pH levels were 2.88 and 4.93. The samples were contained in sealed vials and agitated for 18 ± 2 hours in a rotary shaker at a velocity of 30 rpm. The leachates were further filtered (0.45 μ m), acidified, and analysed by AAS (PerkinElmer PinAAcle 900T) (Gencel et al., 2020).

RESULTS AND DISCUSSION

Characterization of the raw materials

Chemical and mineralogical composition of the raw materials

The clay is mainly composed by SiO_2 (53.72%), Al_2O_3 (23.46%) and appreciable quantities of Fe_2O_3 (5.73%) (Table 1). The SiO_2 content varies generally between 45 and 60% for clay bricks; being one of the main components of bricks (Semiz et al., 2017). The Fe_2O_3 , CaO_3 , CaO_3 and CaO_3 act as effective fluxes reducing the temperature required to form a vitreous material in the body of the bricks, as well as lowering the melting point of the clay (Ravisankar et al., 2010). The clay is considered to be non-calcareous with low refractory properties (Benahsina et al., 2021).

The IMW has SiO₂, Al₂O₃, Fe₂O₃ and CaO contents 49.29, 9.31, 14.67 and 10.06 wt.%, respectively being comparable to that of the clay showing (Table 1). The high Fe₂O₃ content is responsible for the dark color of the Iron Mining Waste (Muñoz et al., 2016) before and after firing. MgO, TiO₂ and Na₂O are present in minor amounts. The most important difference between clay and IMW is the loss on ignition (LOI). Thus, LOI of IMW (13.75 wt.%) is higher than that of clay (10.36 wt.%), due to the presence of abundant carbonates and iron-oxy-hydroxides and organic matter. The inclusion of organic matter in a specific quantity is advantageous for enhancing the mixture's plasticity (Achik et al., 2021).

Mineralogical analysis of the two materials (Fig. 2, Table 1) showed that the IMW contains mainly quartz (23 wt.%), kaolinite (16 wt.%), illite (13 wt.%), calcite (24 wt.%), goethite (16 wt.%), dolomite (3 wt.%) and hematite (3 wt%). The clay is mainly composed of

kaolinite (43wt.%), illite (20 wt.%), quartz (15 wt.%), orthoclase (5 wt.%), calcite (3 wt.%), dolomite (4 wt.%) and goethite (4 wt.%).

Atterberg's Limit of the raw materials

The Plastic Limit is much higher for IMW sample than for the clay sample (Table 2). This could be due to the fact that IMW is richer in fine particles (Gueffaf et al., 2020; Gencel et al., 2020). However, the clay sample exhibited Plasticity Index (PI) value higher than the IMW sample (Table 2); the latter is considered as medium plastic material which requires lesser amount of water to be plastic. Compared to the standard index (ASTM., 2017), IMW is characterized by a medium plasticity.

Thermal behavior of the raw materials (TGA/DSC)

The thermal behavior of IMW sample (Fig. 3a) shows mass loss of 1 and 2.5 wt.% at 25-100 and 250-300 °C respectively; these mass losses are attributed respectively to the loss of moisture and to the dehydration of goethite phase (α -FeO(OH)) featured by an endothermic peak centered at 274 °C (Rizov et al., 2012). Moreover, a mass loss of 1.2 wt. % was recorded at ~ 490 °C featured by a weak endothermic peak, ascribed to the dehydroxylation of kaolinite and illite. Finally, the weight loss of 9 wt% associated with an endothermic peak at 783 °C is attributed to the decomposition of carbonates.

The clay displays a weight loss of 1% at 25-100 °C (Fig. 3b), with an endothermic peak centered at approximately 70 °C attributed to the loss of moisture. Furthermore, a mass loss of 1.7 wt. % at ~ 320 °C; is probably attributed to the combustion of organic matter. The dehydroxylation of kaolinite and illite was recorded by and endothermic peak centered at 513 °C with 7.5 % wt. loss (Mendes et al., 2019). Finally, a weak exothermic peak is observed at 900-910 °C attributed to structural reorganization of metakaolinite (Slimanou et al., 2020). The total weight loss from 25-1000 °C is 13.7 and 10.2 wt.%, for the IMW and the clay respectively.

Physico-chemical characterization of the bricks
Physical characteristics of the bricks

The bricks obtained with various IMW additions fired at 850 and 950 °C show no defects such as cracks, efflorescence or swelling. However, with increasing IMW content, the color of the bricks becomes darker. For samples MB40 and MB50, the red to brown color of the products fired at temperatures of 850 and 950 °C, is due to the high iron oxide content, known as red pigment besides the oxidation of Fe²⁺ to Fe³⁺ (Bouzidi et al., 2014). Additionally, although MnO content is low (~ 1 wt.%) in the IMW (Table 2), it is sufficient to modify the color of the brick producing brown to black hues and improves the surface texture (Bautista-Marín et al., 2021).

Total linear shrinkage reflects the contraction or expansion during the thermal treatment of the fired bricks. Contraction is primarily associated with the formation of the vitreous phase during firing, leading to densification through the filling of voids in the porous structure of the clay-bricks. For standard clay bricks, linear shrinkage is below 8% and when it is higher it leads to deformation of the fired bricks (Pitak et al., 2020; Xin et al., 2021). Total linear shrinkage (Table 3) varies from 4.15 to 7.52% and from 4.92 to 7.74% for the bricks fired at 850 and 950 °C, respectively. Moreover, it varies from 6.95 to 7.32 % for the reference bricks (MB0) fired at 850 and 950 °C, respectively. This is linked to the loss of moisture and adsorbed water between clay particles and in the microstructure of the clay (Phonphuak et al., 2016). However, total linear shrinkage decreased slightly with increasing amount of IMW from 10 to 30 wt %, to 4.15 and 4.92% at both firing temperatures (850 and 950 °C). This is due to the decrease of clay content and the increase of quartz present in the IMW. Quartz functioned as a degreasing agent in the mixture, mitigating potential contraction of the brick body. Moreover, the presence of quartz particles in the iron waste decreased linear shrinkage due to the β-quartz to α-quartz transition for bricks containing less than 30 wt% IMW.

With increasing IMW content above 30 wt %, linear shrinkage increased from 19.2 to 33.42 and from 26.51 to 35.6 % for the bricks fired at 850 and 950 °C respectively. This is probably due to the dehydoxylation of the clay fraction (kaolinite and illite), beside the dehydroxylation of goethite and the collapse of carbonate structure (calcite and dolomite) and dissipation of gases living place to the pore formation (Mekki et al., 2008; Francisco et al., 2019).

The apparent density of bricks fired at 950 °C was higher than those fired at 850 °C and varied as a function of the IMW additions from 1.73 to 2.07 g/cm³ and from 1.76 to 2.26 g/cm³ for the bricks fired at 850 and 950 °C, respectively (Table 3). The apparent density of

the reference bricks was lower than those with IMW addition at both firing temperatures. Thereafter, it increased as with increasing IMW additions (up to 30 wt%) and then it decreased for the samples MB40 and MB50.

On the other hand, the presence of excessive Fe₂O₃ beside K₂O, Na₂O, MnO decreased viscosity of the liquid phase filling the pores and facilitating development of glassy phase that occupies the pores of the fired bricks decreasing open porosity (Sutcu et al., 2016; Phonphuak et al., 2016; Baziz et al., 2019), thereby increasing density. Thereafter, as the IMW content exceeded 30 wt%, apparent density decreased at both firing temperatures showing an increase of water absorption and total linear shrinkage. Moreover, dehydroxylation of kaolinite, illite and goethite and release of gases after firing formed pores and decreased density of the fired bricks. Addition of IMW created a less homogeneous structure where iron particles formed aggregates that increased voids leading to higher absorption and porosity rates (Kandymov et al., 2023).

Apparent porosity and water absorption followed a similar trend for all the bricks (Table 3). Both properties decreased with increase of temperature and IMW content up to 30 wt.%. However, there was a pronounced increase of both parameters when 40 and 50 wt.% of IMW were added in the mixtures which still were lower than the reference bricks (MB0). Addition of 30 wt.% of IMW considerably decreased apparent porosity and water absorption up to 18.04 and 10.14 %, respectively for the bricks fired at 950 °C. This is due to the iron oxides (Fe₂O₃) and alkali oxides (K₂O, Na₂O), which facilitate the development of a glassy phase that occupies the pores of the fired bricks at 850 and 950 °C (Phonphuak et al., 2016). *Mineralogical analysis of the fired clay bricks*

The main phases of bricks fired at 850 °C are quartz, hematite, gehlenite ((2CaO.Al₂O₃.SiO₂) and anorthite (Fig. 4.a); these phases increased as function of IMW additions. However, anorthite formed as a metastable solid solution from phase transformation of calcite and aluminosilicates (CaO-Al₂O₃-SiO₂ system) in the sample MB30 (DeCeanne et al., 2022). At 950 °C, quartz, hematite, gehlenite and anorthite were the main mineralogical phases of the fired bricks; but their intensities slightly diminished compared to bricks fired at 850 °C (Fig. 4.b). Moreover, intensity of quartz peaks of sample MB30 decreased whereas intensity of peaks of hematite, gehlenite and anorthite increased. This might be due to the formation of a glassy phase in MB30 sample, facilitated by the presence of fluxing agents. The Fe₂O₃ along with K₂O and Na₂O are fluxing agents to form a glassy phase at lower temperature (Maniatis et al., 1978; Klaarenbeek., 1961). When the addition of IMW exceeded 30 wt %, the bricks

fired at both temperatures (850 and 950 °C) acquired more porous structure, due to the excessive clay, goethite and calcite contents, that increased water absorption, porosity and total shrinkage rate (Table 3). Moreover, as the amount of refractory oxides (Al₂O₃, MgO) increased, the firing temperatures used in this study are insufficient to decrease the viscosity of the liquid phase, which fill the pores and facilitates formation of glassy phase that fills the pores of the fired bricks. The peaks of quartz and hematite slightly increased in samples MB40 MB50 when the samples were fired 950 °C. and at

FTIR characterization of the bricks

All the samples show weak doublet bands at 1647 and 1552 cm⁻¹ (Fig. 5a, b), attributed to the bending and stretching vibration, due the presence of adsorbed water molecules (Ravisankar et al., 2010). A weak band at ~1416 cm⁻¹ characteristic of carbonates is present in all samples fired at 850 and 950 °C. The 1062-1088 cm⁻¹ absorption bands represent asymmetric Si-O stretching of the main silicate tetrahedral vibrations (Bahçeli et al., 2016). The excessive broadening of absorption bands in the 1100-1000 cm⁻¹ range are attributed to disorder within the tetrahedral sites, leading to the expansion of the Si-O stretching band (Ravisankar et al., 2010). The weak shoulder absorption bands in the range of 916-922 cm⁻¹ observed in the bricks fired at 850 °C (MB30, MB40 and MB50) are due to Al-OH flexure vibrations of phyllosilicates (Terra et al., 2015). These vibrations were retained in samples MB40 and MB50 fired at 950 °C. Additionally, the weak shoulder at 870 cm⁻¹ is observed for the MB30, MB40 and MB50 samples fired at 850 °C, is attributed to FeAlOH vibration present in the IMW (Eliche-Quesada et al., 2017). However, this shoulder band is absent for the samples MB0, MB10 and MB20. On other hand, the weak band at 870 cm⁻¹ is present in MB40 and MB50 samples. The weak bands observed at 784 and 760 cm⁻¹ observed in all the samples are attributed to the Si-O symmetrical stretching vibrations of quartz (Barua., 2003; Namduri et al., 2008). However around The weak shoulder observed at 688 cm⁻¹ in all the samples, is attributed to Si-O symmetrical bending vibrations due the Al for Si substitution. In the 550-570 cm⁻¹ region, a medium intensity band is observed in the FTIR spectrum of all the samples except MB0 and MB10 fired at 850 and 950 °C (Fig. 5a,b). The band is ascribed to Fe-O deformation of hematite (Adazabra et al., 2017).

Microstructure of the fired bricks

The textural characteristics and the evolution of the surface porosity with the firing temperature (850 and 950 °C) have been investigated by Scanning Electron Microscopy

(SEM). Fig. 6 shows the SEM observations of the surface of the bricks with 0, 30 and 40 wt% IMW fired at 850 °C (MB0; MB30 and MB40 respectively). Sample MB0 exhibits high porosity (open and closed pores) and calcite and quartz particles not yet fused (Fig. 6a). Moreover, some agglomerates of fine particles of clay and iron particles are evidenced on the surface of all bricks that have not experienced dehydroxylation. As the amount of the IMW increased to 30 wt%, the morphology of the bricks changed; structure became denser and pores are less abundant than the MB0-850 sample (Fig. 6b). Some kaolinite, quartz and calcite particles along with agglomerates still appear on the matrix of the bricks. The microstructure of the sample containing 40 wt% IMW (Fig. 6c) presented excessive pores and some microcracks due to hydration of CaO during calcination (Cultrone et al., 2004); this involves an increase of porosity, total linear shrinkage and a decrease of the density (Table 3).

As the sintering temperature increased to 950 °C, addition of IMW modified the microstructure of the specimens, leading to densification of the bricks and reduction of porosity with heterogeneous phase distribution and visible closed porosity (Fig. 6d,e,f). This process involves decrease of total linear shrinkage and open porosity observed on sample MB30. In all the bricks, the mineralogical transformations were not coupled by phase consolidation. Moreover, the formation of interconnected grains and glassy phase surrounding grain boundaries are evidenced on the samples MB30 and MB40. Agglomerates of particles embedded on a glassy phase are shown on Figures 6e and 6f. The high Fe₂O₃ content of the waste plays a role of fluxing agent for the mixture (Baziz et al., 2021). Overall, the incorporation of large amounts of IMW (40-50 wt%) resulted in an interlinked pore architecture, as is indicated by the water absorption data (Slimanou et al., 2020).

Mechanical and thermal properties of the fired bricks

Compressive strength

Compressive strength of the reference bricks fired at 850°C and 950°C was 25.95 ± 0.58 MPa and 27.53 ± 0.42 MPa respectively (Fig. 7). Values exhibited an almost linear increase with the incorporation of 30 wt.% IMW for bricks fired at 850 and 950 °C, reaching peak values of 51.84 ± 0.64 MPa and 59.17 ± 0.52 MPa at 850 and 950 °C respectively. This increase is due to the reduction of porosity involving an increase of density. Moreover, hematite and alkali oxides lowered the fusion point of the bricks and hence promoted the liquid phase cementing the crystalline phase in the matrix (James., et al., 1976; Sedmale et al., 2006; Allegretta et al., 2016).

With further increase of IMW addition, compressive strengths of the bricks decreased from 32.11 ±0.57 to 30.22 ±0.65 MPa and from 37.58±0.69 to 31.65±0.52 MPa for the bricks fired at 850 and 950 °C containing 40 and 50 wt. % IMW, respectively. This is due to the increase of water absorption (Table 3) and porosity of the bricks because of their excessive content of clay and quartz phases (Fig. 4, 5) which need higher firing temperature for sintering and consolidation (Coletti et al., 2016). On the other hand, the increase of quartz and hematite content in the bricks could affect negatively the compressive strength since they could lead to the heterogeneity structures and micro-cracks (Monteiro et al., 2004; Souza et al., 2008). Overall, the compressive strength of all the bricks fired at 850 and 950 °C was much higher than the conventional bricks, which have a minimum compressive strength of 10 MPa (Slimanou et al., 2020).

Flexural strength

The construction industry considers the flexural strength of fired bricks as the main quality factor required to assess its suitability (Semiz et al., 2017). The ASTM C67 requires that flexural strength of fired bricks exceeds 2.5 MPA (Dos Reis et al., 2020). In the present study flexural strengths increased as function of IMW addition up to 30 wt.% after firing at 850 and 950 °C (Fig. 8). Reference bricks exhibited values varying from 1.36±0.16 and 3.28±0.10 MPa at 850 and 950 °C, respectively. The flexural strength of the fired bricks varied from 1.36±0.16 to 7.13±0.22 MPa and from 3.28±0.10 to 10.06±0.11 MPa at 850 and 950 °C respectively. Increasing of firing temperature, lead to an increase of flexural strength.

Optimum flexural strength is attained when the bricks contain 30 wt.% IMW (7.13±0.22 and 10.06±0.11 MPa at 850 and 950 °C respectively). This is due to the improvement of vitrification and/or consolidation when the firing temperature increased. However, above 30 wt. % addition of IMW flexural strength decreased to 2.95±0.21 MPa. The decline of mechanical characteristics is attributed to porosity and water absorption, which escalated after addition of IMW.

Thermal conductivity

Materials with low thermal conductivity are superior insulators and help reduce heat loss or gain in buildings. It was therefore crucial to acquire bricks with optimal mechanical and thermal properties. Indeed, standard red bricks have a thermal conductivity of 0.6 Wm-¹

K⁻¹, while insulating bricks have lower thermal conductivity, 0.15 Wm⁻¹ K⁻¹ (Kreimeyer et al., 1987).

The thermal conductivity of bricks fired at 850 and 950 °C increased as function of IMW up to 30 wt% additions (Fig. 9). The thermal conductivities of reference bricks were 0.45±0.02 and 0.47±0.01 Wm⁻¹ K⁻¹, and the bricks with 30 wt % IMW had slightly higher thermal conductivity, namely 0.54±0.03 and 0.56±0.03 Wm⁻¹ K⁻¹ at 850 and 950 °C respectively. This is attributed to the lower porosity of the bricks, which influenced their thermal properties. Addition of IMW up to 30 wt% increased the bulk density and thermal conductivity of the bricks at both firing temperatures. Further addition, 40 to 50 wt% IMW, in the brick specimens caused a slight decrease of thermal conductivity and density due to the increased porosity. This is attributed to air present in pore voids which has a low thermal conductivity (0.024 Wm⁻¹ K⁻¹) acting as thermal insulator (Kadir et al., 2015; Wang et al., 2024).

Environmental assessment

According to the results of the toxicity characteristics (TCLP) of the bricks with 0, 10, 20, 30 and 40 wt% IMW (Table 4), the heavy metal concentrations of all the bricks decreased with increasing firing temperature from 850 to 950 °C. The concentration of Zn and Ni is higher in the reference bricks than in the bricks with the IMW, probably because that the clay contains higher content of Zn and Ni. On the other hand, Pb and Fe concentrations remain higher in the bricks with IMW than in the reference bricks. During firing, the heavy metals are trapped and immobilized in the glassy phase composing the bricks structure in both firing temperatures. Overall, the results of these experiments were below the limits set by the USEPA (Chen et al., 1988).

In this study, 30wt% of IMW could be used as raw material to produce clay bricks; the bricks had compressive strengths of 51.84±0.64 and 59.17±0.52 MPa, and thermal conductivity of 0.45 ±0.01 and 0.5± 0.02 after firing at 850 and 950 °C respectively. These results are comparable to those of (Beartyz et al., 2020), reporting the feasibility of adding IMW to fired bricks in proportions ranging from 0 to 50%. Addition of IMW reduces linear shrinkage and compressive strength during firing. Nevertheless, addition of 20 wt. % of IMW is considered acceptable to maintain quality in line with fired brick standards. Chen et al (2011) showed that bricks obtained by mixing 84% IMW, 10% clay and 6% fly ash fired at 980-1030 °C complied with the Chinese standard. In addition, water absorption of 16.54 to 17.93% and compressive strength of 20.03 to 22.92 MPa were observed, also satisfying the requirements of the standard. In conclusion, IMW offer a promising alternative in the

manufacture of fired bricks, with satisfactory physical and mechanical properties and minimal environmental impact.

SUMMARY AND CONCLUSIONS

This study examined the use of as-received IMW for the production of fired clay bricks. Different proportions of IMW (0, 10, 20, 30, 40 and 50 wt%) were added to the bricks. Physical, mechanical and thermal properties, the microstructure and environmental impact were evaluated. Based on the results of this study, the following conclusions can be drawn:

The IMW has a high concentration of Fe_2O_3 and SiO_2 and silica and contains abundant kaolinite (16%), illite (13%), quartz (23%), goethite (16%) and calcite (24%) and minor hematite (3%) and dolomite (3%).

Total shrinkage, water absorption and porosity are significantly reduced by increasing the amount of IMW up to 30% to brick composition, at both firing temperatures (850 and 950°C). This is due to the decrease of clay content and the increase of quartz with addition of the IMW. Brick density increased with firing temperature (950 °C) and IMW addition, up to 30 wt%, due to the formation of liquid phase, promoted by the Fe₂O₃ content, which filled the internal pores and reduced open porosity. On the other hand, when IMW exceeded 30 wt%, the density decreased while the open porosity and water absorption increased, because the sintering temperature (950°C) was not sufficient to form a glass phase. The water absorption of all bricks was below 20 wt% meeting the ASTM standards for bricks.

The main phases of bricks at 850 °C are quartz, hematite, gehlenite and anorthite, the abundance of which increased with the addition of IMW. However, anorthite appeared as a metastable solid solution resulting from the phase transformation of calcite and aluminosilicate phases in sample MB30. Additionally, the bricks fired at 950°C have the same phases, although less abundant compared to bricks fired at 850°C.

All samples showed mechanical strength values in excess of the required standards, with compressive strength of 25.95 and 27.53 MPa after firing at 850 and 950°C respectively. When the optimum (30 wt%) addition of IMW is added, compressive and flexural strengths of the bricks increased from 51.84 to 59.17 MPa and from 7.13 to 10.06 MPa respectively for the bricks fired at 850 and 950°C. This is due to densification and elimination of open porosity. The presence of Fe₂O₃, Na₂O, K₂O and MnO decreased the temperature of liquid

that involves formation of the glassy phase after cooling. The decline in mechanical characteristics with the incorporation of 40% and 50% IMW is attributed mostly to higher porosity and water absorption after addition of IMW.

Thermal conductivity increased with the incorporation of IMW after firing at 850 and 950°C. Brick samples with 30 wt% of IMW show thermal conductivity values of 0.54 and 0.56 Wm⁻¹K⁻¹. Minimum thermal conductivity achieved was 0.45 and 0.47 Wm⁻¹K⁻¹ for the control bricks fired at 850 and 950°C, respectively. The results of the TCLP leaching test showed that the heavy metals are trapped during firing and immobilized in the glassy phase that makes up the brick structure at both firing temperatures. Results for all samples were below USEPA limits.

Iron Mining Waste can be successfully recycled in and met all current standards for brick making. In this case study, the optimum amount of IMW was 30 wt% giving maximum values of mechanical strength and acceptable values of thermal conductivity with less open porosity. Therefore, fired bricks production in the range of temperature of 850 and 950°C incorporating IMW could be a substantial step towards a decrease in pollution and environmental impact which contribute to sustainable development and circular economy principles.

Acknowledgments

The authors want to thank the Center for Scientific and Technical Research in Physico-Chemical Analysis of Bejaia, Algeria (CRAPC). Our recognition to El Ouenza mine who provides us the Iron Mining Waste samples.

References

Achik, M., Benmoussa, H., Oulmekki, A., Ijjaali, M., el Moudden, N., Touache, A., Álvaro, G. G., Rivera, F. G., Infantes-Molina, A., Eliche-Quesada, D., & Kizinievic, O. (2021). Evaluation of technological properties of fired clay bricks containing pyrrhotite ash. *Construction and Building Materials*, 269. https://doi.org/10.1016/j.conbuildmat.2020.121312

Adazabra, A. N., Viruthagiri, G., & Shanmugam, N. (2017). Infrared analysis of clay bricks incorporated with spent shea waste from the shea butter industry. *Journal of Environmental Management*, 191.https://doi.org/10.1016/j.jenvman.2017.01.006

Ahmad, S., Iqbal, Y., & Muhammad, R. (2017). Effects of coal and wheat husk additives on the physical, thermal and mechanical properties of clay bricks. *Boletin de La Sociedad Espanola de Ceramica y Vidrio*, *56*(3). https://doi.org/10.1016/j.bsecv.2017.02.001

Allegretta, I., Pinto, D., & Eramo, G. (2016). Effects of grain size on the reactivity of limestone temper in a kaolinitic clay. *Applied Clay Science*, *126*. https://doi.org/10.1016/j.clay.2016.03.020

ASTM D4318-17e1. (2017). Standard Test Methods for Liquid Limit, Plastic Limit, and Plasticity Index of Soils, ASTM International, West Conshohocken, PA.

Baala, D., Idres, A., Bounouala, M., &Benselhoub, A. (2018). Radiometric sorting techniques for mining wastes from Ouenza iron mine (Algeria). Scientific Bulletin of National Mining University, (5). DOI: 10.29202/nvngu/2018-5/3

Bahçeli, S., Güleç, G., Erdolan, H., & Sölüt, B. (2016). Micro-Raman and FT-IR spectroscopic studies of ceramic shards excavated from ancient Stratonikeia city at Eskihisar village in West-South Turkey. *Journal of Molecular Structure*, 1106. https://doi.org/10.1016/j.molstruc.2015.10.036

Bai, M., Xiao, J., Gao, Q., & Shen, J. (2023). Utilization of construction spoil and recycled powder in fired bricks. *Case Studies in Construction Materials*, 18. https://doi.org/10.1016/j.cscm.2023.e02024

Barua, A. G., Boruah, B. R., Bhattacharyya, S., & Baruah, G. D. (2003). Spectroscopic investigation of the dergaon meteorite with reference to 10 μm and 20 μm bands. *Pramana - Journal of Physics*, 60(1). https://doi.org/10.1007/BF02705067

Bautista-Marín, J. D., Esguerra-Arce, A., & Esguerra-Arce, J. (2021). Use of an industrial solid waste as a pigment in clay bricks and its effects on the mechanical properties. Construction and Building Materials, 306, 124848.

Baziz, A., Bouzidi, N., & Eliche-Quesada, D. (2021). Recycling of gold mining reject from Amesmessa mine as ceramic raw material: microstructure and mechanical properties.

Environmental Science and Pollution Research, 28(34). https://doi.org/10.1007/s11356-020-12017-y

Benahsina, A., Taha, Y., Bouachera, R., Elomari, M., & Bennouna, M. A. (2021). Manufacture and characterization of fired bricks from gold mine waste rocks. *Minerals*, *11*(7). https://doi.org/10.3390/min11070695

Boutarfa, F., Idres, A., Mekti, Z., Graine, R., Tiour, F., Dovbash, N., Benselhoub, A., & Bellucci, S. (2023). Airborne dust pollution emitted by El Hadjar Metallurgical Complex: quantification, characterization, and occupational health hazards. *Technology Audit and Production Reserves*, 5(3(73)). https://doi.org/10.15587/2706-5448.2023.289353

Bouzeriba, H., Bouzidi, N., Idres, A., Laala, I., &Zaoui, L. (2025). Feasibility assessment of low-grade iron ore from El Ouenza mine by high-intensity magnetic separation. Natsional'nyiHirnychyiUniversytet.NaukovyiVisnyk, (1), 28-33.https://doi.org/10.33271/nvngu/2025-1/028

Božič, M., Žibret, L., Kvočka, D., Pranjić, A. M., Gregorc, B., & Ducman, V. (2023). Drava river sediment in clay brick production: Characterization, properties, and environmental performance. *Journal of Building Engineering*, 71. https://doi.org/10.1016/j.jobe.2023.106470 Chen, M., & Ma, L. Q. (1998). Comparison of Four USEPA Digestion Methods for Trace Metal Analysis Using Certified and Florida Soils. *Journal of Environmental Quality*, 27(6). https://doi.org/10.2134/jeq1998.00472425002700060004x

Chen, Y., Zhang, Y., Chen, T., Zhao, Y., & Bao, S. (2011). Preparation of eco-friendly construction bricks from hematite tailings. *Construction and building materials*, 25, 2107-2111. https://doi.org/10.1016/j.conbuildmat.2010.11.025

Coletti, C., Cultrone, G., Maritan, L., & Mazzoli, C. (2016). How to face the new industrial challenge of compatible, sustainable brick production: Study of various types of commercially available bricks. *Applied Clay Science*, 124–125. https://doi.org/10.1016/j.clay.2016.02.014

Cultrone, G., Sebastián, E., Elert, K., de la Torre, M. J., Cazalla, O., & Rodriguez-Navarro, C. (2004). Influence of mineralogy and firing temperature on the porosity of bricks. *Journal of the European Ceramic Society*, 24(3). https://doi.org/10.1016/S0955-2219(03)00249-8

Dabaieh, M., Heinonen, J., El-Mahdy, D., Hassan, D. M. (2020). A comparative study of life cycle carbon emissions and embodied energy between sun-dried bricks and fired clay bricks. *Journal of Cleaner Production*, 275. https://doi.org/10.1016/j.jclepro.2020.122998

DeCeanne, A. v., Rodrigues, L. R., Wilkinson, C. J., Mauro, J. C., & Zanotto, E. D. (2022). Examining the role of nucleating agents within glass-ceramic systems. In *Journal of Non-Crystalline Solids* (Vol. 591). https://doi.org/10.1016/j.jnoncrysol.2022.121714

Detho, A., Kadir, A. A., & Ahmad, S. (2024). Utilization of wastewater treatment sludge in the production of fired clay bricks: An approach towards sustainable development. *Results in Engineering*, 21. https://doi.org/10.1016/j.rineng.2023.101708

Dos Reis, G. S., Cazacliu, B. G., Cothenet, A., Poullain, P., Wilhelm, M., Sampaio, C. H., Lima, E. C., Ambros, W., & Torrenti, J. M. (2020). Fabrication, microstructure, and properties of fired clay bricks using construction and demolition waste sludge as the main additive. *Journal of Cleaner Production*, 258. https://doi.org/10.1016/j.jclepro.2020.120733

Dubale, M., Goel, G., Kalamdhad, A., & Singh, L. B. (2022). An investigation of demolished floor and wall ceramic tile waste utilization in fired brick production. *Environmental Technology and Innovation*, 25. https://doi.org/10.1016/j.eti.2021.102228

Eliche-Quesada, D., Martínez-García, C., Martínez-Cartas, M. L., Cotes-Palomino, M. T., Pérez-Villarejo, L., Cruz-Pérez, N., & Corpas-Iglesias, F. A. (2011). The use of different forms of waste in the manufacture of ceramic bricks. *Applied Clay Science*, *52*(3). https://doi.org/10.1016/j.clay.2011.03.003

Eliche-Quesada, D., Sandalio-Pérez, J. A., Martínez-Martínez, S., Pérez-Villarejo, L., & Sánchez-Soto, P. J. (2018). Investigation of use of coal fly ash in eco-friendly construction materials: fired clay bricks and silica-calcareous non fired bricks. *Ceramics International*, 44(4). https://doi.org/10.1016/j.ceramint.2017.12.039

Ettoumi, M., Jouini, M., Neculita, C. M., Bouhlel, S., Coudert, L., Taha, Y., & Benzaazoua, M. (2021). Characterization of phosphate processing sludge from Tunisian mining basin and its potential valorization in fired bricks making. *Journal of Cleaner Production*, 284. https://doi.org/10.1016/j.jclepro.2020.124750

Francisco M. Fernandes."Clay bricks- Long-term Performance and Durability of Masonry Structures", Woodhead Publishing Series in Civil and Structural Engineering, 2019, Pages 3-19

G. Sedmale, I. Sperberga, U. Sedmalis, Z. Valancius, Formation of hightemperature crystalline phases in ceramic from illite clay and dolomite, J. Eur. Ceram. Soc. 26 (2006) 3351–3355. https://doi.org/10.1016/j.jeurceramsoc.2005.10.012

Galán-Arboledas, R. J., Cotes-Palomino, M. T., Bueno, S., & Martínez-García, C. (2017). Evaluation of spent diatomite incorporation in clay based materials for lightweight bricks processing. *Construction and Building Materials*, 144. https://doi.org/10.1016/j.conbuildmat.2017.03.202

Hafez, R. D. A., Tayeh, B. A., & Abd- Al Ftah, R. O. (2022). Development and evaluation of green fired clay bricks using industrial and agricultural wastes. *Case Studies in Construction Materials*, 17. https://doi.org/10.1007/BF00375418

Hussien, A., Al Zubaidi, R., Jannat, N., Ghanim, A., Maksoud, A., Al-Shammaa, A. (2024). The effects of tea waste additive on the physical and mechanical characteristics of structural unfired clay bricks. Alex. Eng. J. *101*, 282-294.https://doi.org/10.1016/j.aej.2024.05.090

Idrees, M., Akbar, A., Saeed, F., Gull, M., & Eldin, S. M. (2023). Sustainable production of Low-Shrinkage fired clay bricks by utilizing waste plastic dust. *Alexandria Engineering Journal*, 68. https://doi.org/10.1016/j.aej.2023.01.040

Idres, A., Bouhedja, A., Bounouala, M., &Benselhoub, A. (2016). New method of electrostatic separation of the oxidized iron ore. Mining Science, 23, 33-41.4. Doi: 10.5277/msc162303

ISO 8894-1:2010. (2010). Refractory materials - Determination of thermal conductivity - Part 1: Hot-wire methods (cross-array and resistance thermometer). *ISO Standard*.

Kadir, A. A., & Mohajerani, A. (2015). Effect of heating rate on gas emissions and properties of fired clay bricks and fired clay bricks incorporated with cigarette butts. *Applied Clay Science*, 104, 269-276. https://doi.org/10.1016/j.clay.2014.12.005

Kandymov, N., Korpayev, S., Durdyev, S., Myratberdiyev, R., &Gurbanmyradova, L. (2023). Manufacturing of Fired Clay Bricks for Internal Walls with Dolomite Residue as a Secondary Material Buildings, 13(12), 3065.

Klaarenbeek, F.W. The development of yellow colors in calcareous bricks, Trans. Br. Ceram. Soc. 60 (1961) 738–772. https://doi.org/10.1016/j.clay.2015.01.017

Kreimeyer, R. (1987). Some notes on the firing colour of clay bricks. *Applied clay science*, 2(2), 175-183. https://doi.org/10.1016/0169-1317(87)90007-X

Lamani, S. R., Mangalpady, A., & Vardhan, H. (2017). Investigating the Utility of Iron Ore Waste in Preparing Non-fired Bricks. *Journal of The Institution of Engineers (India): Series D*, 98(2). https://doi.org/10.1007/s40033-016-0129-5

Lang, L., Chen, B., & Pan, Y. (2020). Engineering properties evaluation of unfired sludge bricks solidified by cement-fly ash-lime admixed nano-SiO2 under compaction forming technology. *Construction and Building Materials*, 259. https://doi.org/10.1016/j.conbuildmat.2020.119879

Li, R., Zhou, Y., Li, C., Li, S., & Huang, Z. (2019). Recycling of industrial waste iron tailings in porous bricks with low thermal conductivity. *Construction and Building Materials*, *213*. https://doi.org/10.1016/j.conbuildmat.2019.04.040

Maafa, I. M., Abutaleb, A., Zouli, N., Zeyad, A. M., Yousef, A., & Ahmed, M. M. (2023). Effect of agricultural biomass wastes on thermal insulation and self-cleaning of fired bricks. *Journal of Materials Research and Technology*, 24. https://doi.org/10.1016/j.jmrt.2023.03.189

Maniatis, Y., Simopoulos, A., & Kostikas, A. (1981). Moessbauer Study of the Effect of Calcium Content on Iron Oxide Transformations in Fired Clays. *Journal of the American Ceramic Society*, 64(5). https://doi.org/10.1111/j.1151-2916.1981.tb09599.x

Mekki, H., Anderson, M., Benzina, M., & Ammar, E. (2008). Valorization of olive mill waste water by its incorporation in building bricks. *Journal of Hazardous Materials*, *158*(2–3). https://doi.org/10.1016/j.jhazmat.2008.01.104

Mendes, B. C., Pedroti, L. G., Fontes, M. P. F., Ribeiro, J. C. L., Vieira, C. M. F., Pacheco, A. A., & Azevedo, A. R. G. de. (2019). Technical and environmental assessment of the

incorporation of iron ore tailings in construction clay bricks. *Construction and Building Materials*, 227. https://doi.org/10.1016/j.conbuildmat.2019.08.050

Mine documentation (2024). The El Ouenza Mine History and Future. Study and Development Division Geology Service.

Monteiro, S. N., & Vieira, C. M. F. (2004). Influence of firing temperature on the ceramic properties of clays from Campos dos Goytacazes, Brazil. *Applied Clay Science*, 27(3–4). https://doi.org/10.1016/j.clay.2004.03.002

Muñoz V., P., Morales O., M. P., Letelier G., V., & Mendívil G., M. A. (2016). Fired clay bricks made by adding wastes: Assessment of the impact on physical, mechanical and thermal properties. In *Construction and Building Materials* (Vol. 125). https://doi.org/10.1016/j.conbuildmat.2016.08.024

Nagaraj, H. B., Sravan, M. v., Arun, T. G., & Jagadish, K. S. (2014). Role of lime with cement in long-term strength of Compressed Stabilized Earth Blocks. *International Journal of Sustainable Built Environment*, *3*(1). https://doi.org/10.1016/j.ijsbe.2014.03.001

Namduri, H., & Nasrazadani, S. (2008). Quantitative analysis of iron oxides using Fourier transform infrared spectrophotometry. *Corrosion Science*, 50(9). https://doi.org/10.1016/j.corsci.2008.06.034

Ozturk, S., Sutcu, M., Erdogmus, E., & Gencel, O. (2019). Influence of tea waste concentration in the physical, mechanical and thermal properties of brick clay mixtures. *Construction and Building Materials*, 217. https://doi.org/10.1016/j.conbuildmat.2019.05.114

Phonphuak, N., Kanyakam, S., & Chindaprasirt, P. (2016). Utilization of waste glass to enhance physical-mechanical properties of fired clay brick. *Journal of Cleaner Production*, 112. https://doi.org/10.1016/j.jclepro.2015.10.084

Pitak, I., Baltušnikas, A., Kalpokaitė-Dičkuvienė, R., Kriukiene, R., & Denafas, G. (2022). Experimental study effect of bottom ash and temperature of firing on the properties, microstructure and pore size distribution of clay bricks: A Lithuania point of view. *Case Studies in Construction Materials*, 17. https://doi.org/10.1016/j.cscm.2022.e01230

R.S. James, A.C. Turnock, J.J. Fawcett, The stability and phase relations of iron chlorite below 8.5 kb P-H20, Contrib. Mineral. Petrol. 56 (1976) 1–25, https://doi.org/10.1007/BF00375418

Rashid, K., Haq, E. U., Kamran, M. S., Munir, N., Shahid, A., & Hanif, I. (2019). Experimental and finite element analysis on thermal conductivity of burnt clay bricks reinforced with fibers. *Construction and Building Materials*, 221. https://doi.org/10.1016/j.conbuildmat.2019.06.055

Rashid, M. I., Benhelal, E., & Rafiq, S. (2020). Reduction of Greenhouse Gas Emissions from Gas, Oil, and Coal Power Plants in Pakistan by Carbon Capture and Storage (CCS): A Review. *Chemical Engineering and Technology*, 43(11). https://doi.org/10.1002/ceat.201900297

Raut, A. N., & Gomez, C. P. (2017). Development of thermally efficient fibre-based eco-friendly brick reusing locally available waste materials. *Construction and Building Materials*, 133. https://doi.org/10.1016/j.conbuildmat.2016.12.055

Ravisankar, R., Kiruba, S., Eswaran, P., Senthilkumar, G., & Chandrasekaran, A. (2010). Mineralogical characterization studies of ancient potteries of Tamilnadu, India by FT-IR spectroscopic technique. *E-Journal of Chemistry*, 7(SUPPL. 1). https://doi.org/10.1155/2010/643218

Rizov, B. (2012). Phase transformations from goethite to hematite and thermal decomposition in various nickeliferous laterite ores. *Journal of the University of Chemical Technology and Metallurgy*, 47(2).

Semiz, B. (2017). Characteristics of clay-rich raw materials for ceramic applications in Denizli region (Western Anatolia). *Applied Clay Science*, 137. https://doi.org/10.1016/j.clay.2016.12.014

Shi, J., Chun, Q., Mi, Z., Feng, S., Liu, C., Liu, Z., Wang, D., & Zhang, Y. (2023). Comparative study on material properties of ancient fired clay bricks of China. *Case Studies in Construction Materials*, *19*. https://doi.org/10.1016/j.cscm.2023.e02463

Silva Ramos, L. T. da, de Azevedo, R. C., Silva Bezerra, A. C. da, do Amaral, L. M., & Oliveira, R. D. (2024). Iron ore tailings as a new product: A review-based analysis of its

potential incorporation capacity by the construction sector. *Cleaner Waste Systems* (Vol. 7). https://doi.org/10.1016/j.clwas.2024.100137

Slimanou, H., Eliche-Quesada, D., Kherbache, S., Bouzidi, N., & Tahakourt, A. /K. (2020). Harbor Dredged Sediment as raw material in fired clay brick production: Characterization and properties. *Journal of Building Engineering*, 28. https://doi.org/10.1016/j.jobe.2019.101085

Souza, C. C. I.; Vieira, C. M. F. I., & Monteiro. (2008). Alterações microestruturais de cerâmica argilosa incorporada com rejeito de minério de ferro Microstructural changes of clayey ceramic incorporated with iron ore tailings. *Revista Matéria*, *v*, *13*(1).

Sutcu, M., Alptekin, H., Erdogmus, E., Er, Y., & Gencel, O. (2015). Characteristics of fired clay bricks with waste marble powder addition as building materials. *Construction and Building Materials*, 82. https://doi.org/10.1016/j.conbuildmat.2015.02.055

Sutcu, M., Erdogmus, E., Gencel, O., Gholampour, A., Atan, E., & Ozbakkaloglu, T. (2019). Recycling of bottom ash and fly ash wastes in eco-friendly clay brick production. *Journal of Cleaner Production*, 233. https://doi.org/10.1016/j.jclepro.2019.06.017

Sutcu, M., Ozturk, S., Yalamac, E., & Gencel, O. (2016). Effect of olive mill waste addition on the properties of porous fired clay bricks using Taguchi method. *Journal of Environmental Management*, 181. https://doi.org/10.1016/j.jenvman.2016.06.023

Terra, F. S., Demattê, J. A. M., & Viscarra Rossel, R. A. (2015). Spectral libraries for quantitative analyses of tropical Brazilian soils: Comparing vis-NIR and mid-IR reflectance data. *Geoderma*, 255–256. https://doi.org/10.1016/j.geoderma.2015.04.017

Thejas, H. K., & Hossiney, N. (2022). Alkali-activated bricks made with mining waste iron ore tailings. *Case Studies in Construction Materials*, 16. https://doi.org/10.1016/j.cscm.2022.e00973

Thomas, G., Isabelle, C., Frederic, H., Catherine, P., & Marie-Anne, B. (2021). Demonstrating the influence of sediment source in dredged sediment recovery for brick and tile production. *Resources, Conservation and Recycling*, 171. https://doi.org/10.1016/j.resconrec.2021.105653

Velasco, P. M., Ortiz, M. P. M., Giró, M. A. M., Melia, D. M., & Rehbein, J. H. (2015). Development of sustainable fired clay bricks by adding kindling from vine shoot: Study of

thermal and mechanical properties. *Applied Clay Science*, 107. https://doi.org/10.1016/j.clay.2015.01.017

Vilela, A. P., Eugênio, T. M. C., de Oliveira, F. F., Mendes, J. F., Ribeiro, A. G. C., Brandão Vaz, L. E. V. de S., & Mendes, R. F. (2020). Technological properties of soil-cement bricks produced with iron ore mining waste. *Construction and Building Materials*, 262. https://doi.org/10.1016/j.conbuildmat.2020.120883

Viruthagiri, G., Sathiya Priya, S., Shanmugam, N., Balaji, A., Balamurugan, K., & Gopinathan, E. (2015). Spectroscopic investigation on the production of clay bricks with SCBA waste. *Spectrochimica Acta - Part A: Molecular and Biomolecular Spectroscopy*, *149*. https://doi.org/10.1016/j.saa.2015.05.006

Wang, C., Wang, J., Li, Q., Xu, S., & Yang, J. (2024). A review on recent development of foam Ceramics prepared by particle-stabilized foaming technique. *Advances in Colloid and Interface Science*, 103198. https://doi.org/10.1016/j.cis.2024.103198

Weishi, L., Guoyuan, L., Ya, X., & Qifei, H. (2018). The properties and formation mechanisms of eco-friendly brick building materials fabricated from low-silicon iron ore tailings. *Journal of Cleaner Production*, 204. https://doi.org/10.1016/j.jclepro.2018.08.309

Xin, Y., Kurmus, H., Mohajerani, A., Dallol, Y., Lao, Y., Robert, D., Pramanik, B., & Tran, P. (2021). Recycling crushed waste beer bottle glass in fired clay bricks. *Buildings*, *11*(10). https://doi.org/10.3390/buildings11100483

Xin, Y., Robert, D., Mohajerani, A., Tran, P., & Pramanik, B. K. (2023). Utilizing rejected contaminants from the paper recycling process in fired clay brick production. *Construction and Building Materials*, 409. https://doi.org/10.1016/j.conbuildmat.2023.134031

Xin, Y., Robert, D., Mohajerani, A., Tran, P., & Pramanik, B. K. (2023). A Viable Solution for Industrial Waste Ash: Recycling in Fired Clay Bricks. *Journal of Materials in Civil Engineering*, 35(8). https://doi.org/10.1061/jmcee7.mteng-15165

Yang, C., Cui, C., Qin, J., & Cui, X. (2014). Characteristics of the fired bricks with low-silicon iron tailings. *Construction and Building Materials*, 70. https://doi.org/10.1016/j.conbuildmat.2014.07.075

Zhang, N., Tang, B., & Liu, X. (2021). Cementitious activity of iron ore tailing and its utilization in cementitious materials, bricks and concrete. *Construction and Building Materials*, 288. https://doi.org/10.1016/j.conbuildmat.2021.123022.

Liste of tables

Table 1: Chemical and mineralogical composition of IMW and clay materials

Oxides		IMW	Clay
SiO ₂		49.29	53.72
Al_2O_3		9.31	23.46
Fe_2O_3		14.67	5.73
CaO		10.06	1.34
MgO		0.53	1.51
K_2O		1.14	2.65
Na_2O		0.13	0.25
MnO		0.97	0.31
TiO_2		0.15	0.67
L.O.I		13.75	10.36
Kaolinite		16	43
illite		13	20
Quartz		23	15
Calcite		24	3
Dolomite		3	4
Orthose		0	5
Goethite	,	16	4
Hematite		3	2
Organic matter		-	2

L.O.I: Loss On Ignition

Table 2: Atterberg's limits of the raw materials

Atterbeg's limits	Clay	Iron Mining Waste		
Plastic Limit, PL(%)	25.70	31.86		
Plasticity Index, PI(%)	26.03	17.16		
Liquid Limit, LL(%)	51.73	49.02		

Table 3: Physical properties of bricks fired at 850 °C and 950 °C.

Bricks	Temperature	Total	Apparent	Bulk	Water	Compressive	Flexural
	(°C)	Linear	porosity	density	Absorption	strength	strength
		Shrinkage	(%)	(g/cm^3)	(%)	(MPa)	(MPa)
		(%)					
MB0	850	6.95	36.32	1.73	17.51	25.95	1.36
		± 0.76	± 1.18	± 1.90	± 0.46	± 0.58	± 0.16
	950	7.32	35.14	1.76	16.13	27.53	3.28
		± 0.58	± 0.92	± 0.96	± 0.11	± 0.42	± 0.10
MB10	850	6.42	33.45	1.80	16.79	33.20	2.39
		± 0.79	± 1.30	± 1.32	± 0.95	±0.40	± 0.54
	950	7.83	32.27	1.82	15.69	35.17	2.73
		± 0.41	± 2.15	± 1.58	± 0.90	±0.48	±0.25
MB20	850	5.08	25.20	1.87	13.19	30.53	4.58
		± 0.82	± 0.60	± 1.20	±0.39	±0.48	± 0.24
	950	6.62	23.07	1.89	12.28	32.43	5.37
		± 0.38	± 0.95	± 1.08	± 0.37	±1.51	± 0.31
MB30	850	4.15	18.85	2.07	10.82	51.84	7.13
		± 0.41	± 0.87	± 1.73	± 0.86	± 0.64	± 0.22
	950	4.92	18.04	2.26	10.14	59.17	10.06
		± 0.79	± 0.77	± 1.40	±0.73	± 0.52	± 0.11
MB40	850	5.32	26.51	1.86	14.34	32.11	5.96
		± 0.50	± 0.49	± 1.89	±0.15	± 0.57	± 0.23
	950	5.87	19.20	2.03	11.61	37.58	8.09
		± 0.56	± 0.97	± 1.03	± 0.92	± 0.69	± 0.28
MB50	850	7.52	35.60	1.74	18.56	30.22	2.95
		±0.39	±0.68	± 0.69	± 0.71	± 0.65	± 0.21
	950	7.74	33.42	1.78	13.21	31.65	5.59
		±0.12	±1.03	± 0.85	±0.36	±0.52	±0.20

Table 4: Leachability of the heavy metals as function of temperature (Concentrations in (mg/L)).

Element	Bricks fired at 850 °C				Bricks fired at 950 °C				Limites US-EPA ^a
	MB0	MB10	MB30	MB40	MB0	MB10	MB30	MB40	_
Zn	0.718	0.515	0.382	0.361	0.541	0.367	0.366	0.340	500
Pb	2.276	3.774	4.466	4.801	1.225	1.453	2.358	2.647	5.0
Ni	0.164	0.127	0.109	0.092	0.114	0.108	0.068	0.043	11
Fe	354.83	393.76	414.70	401.83	173.15	239.86	264.20	314.84	-

^a United States Environmental Protection Agency (USEPA) (1996).

Figure captions

Figure.1: Simplified diagram illustrating the manufacture of bricks.

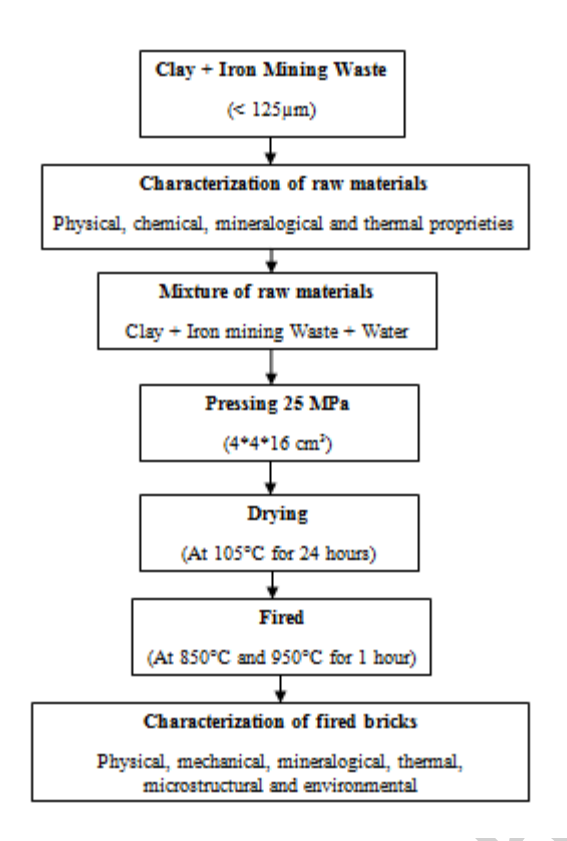


Figure.2: XRD traces of the raw materials (**K:** Kaolinite; I: illite; Q: Quartz; C: Calcite D: Dolomite; G: goethite; H: Hematite; T: Todorokite).

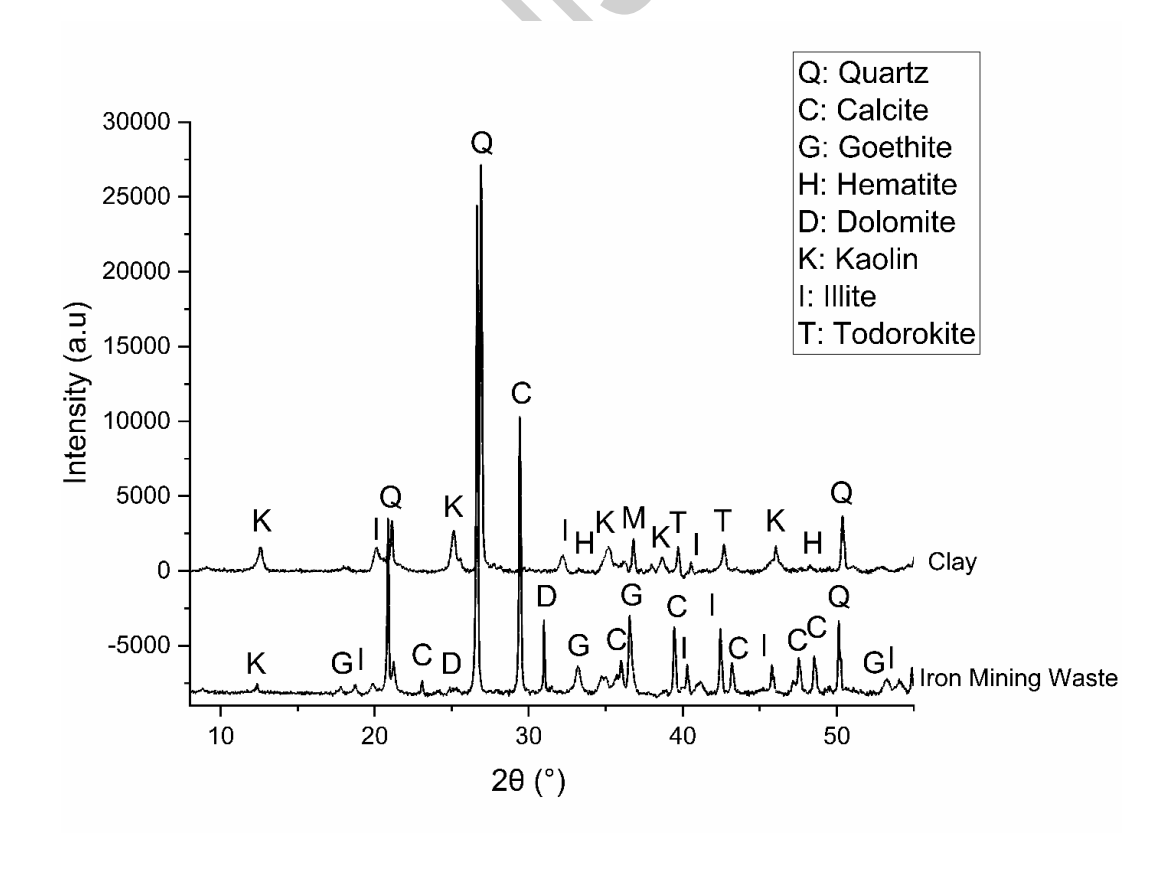


Figure.3: TGA and DSC curve of the raw materials: (a) IMW and (b) Clay.

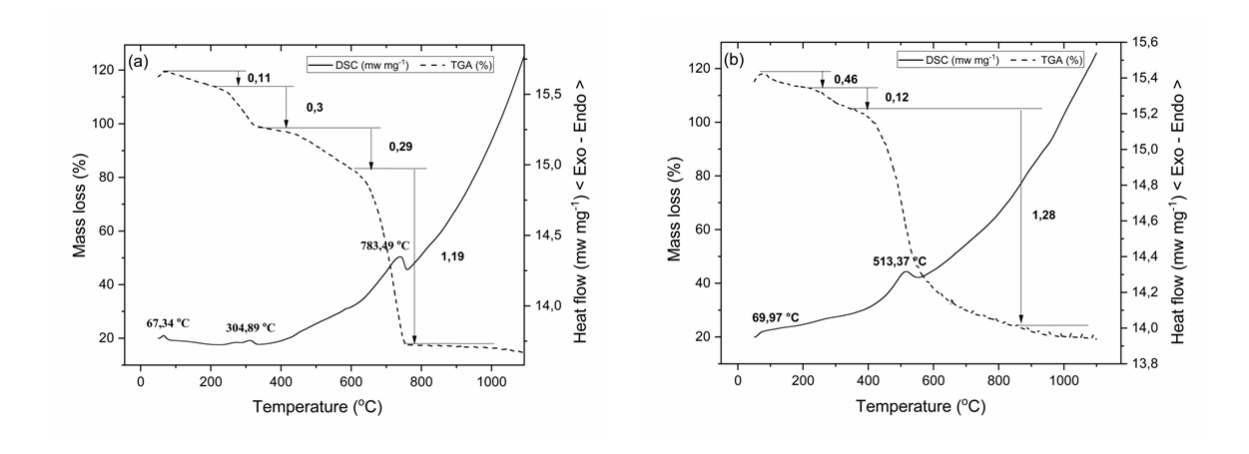


Figure.4: XRD traces of bricks fired at (a) 850 °C and (b) 950 °C

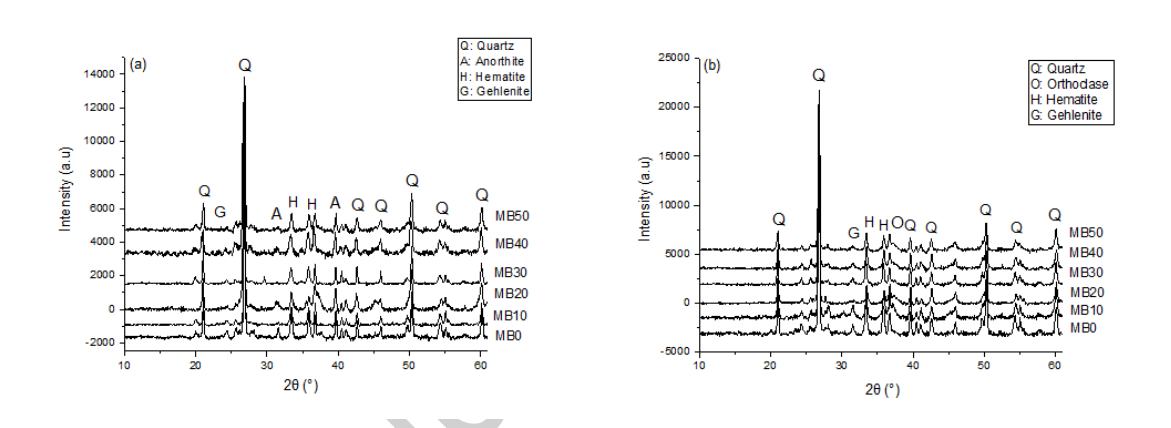


Figure.5: FTIR spectra of bricks fired at (a) 850 °C, and (b) 950 °C.

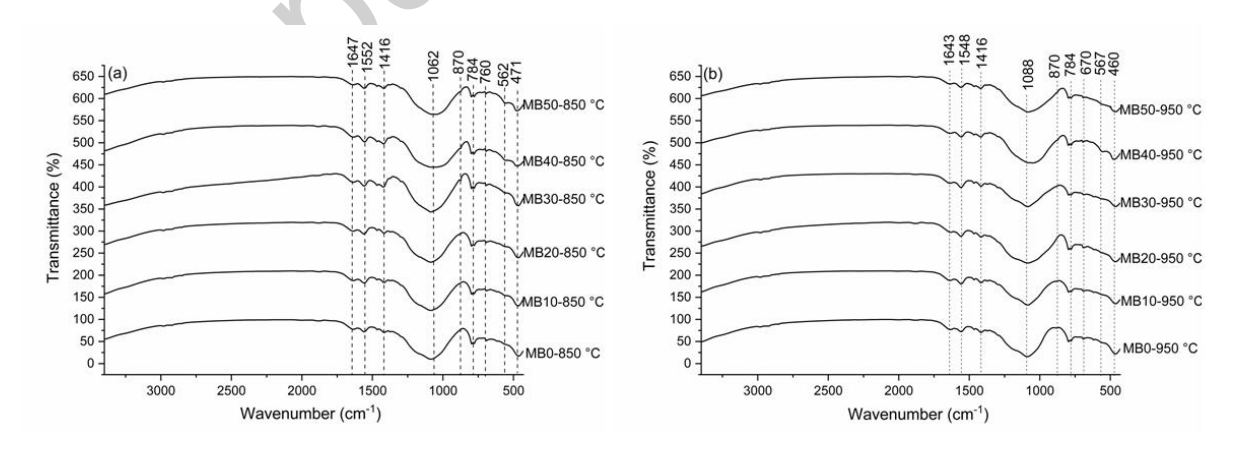
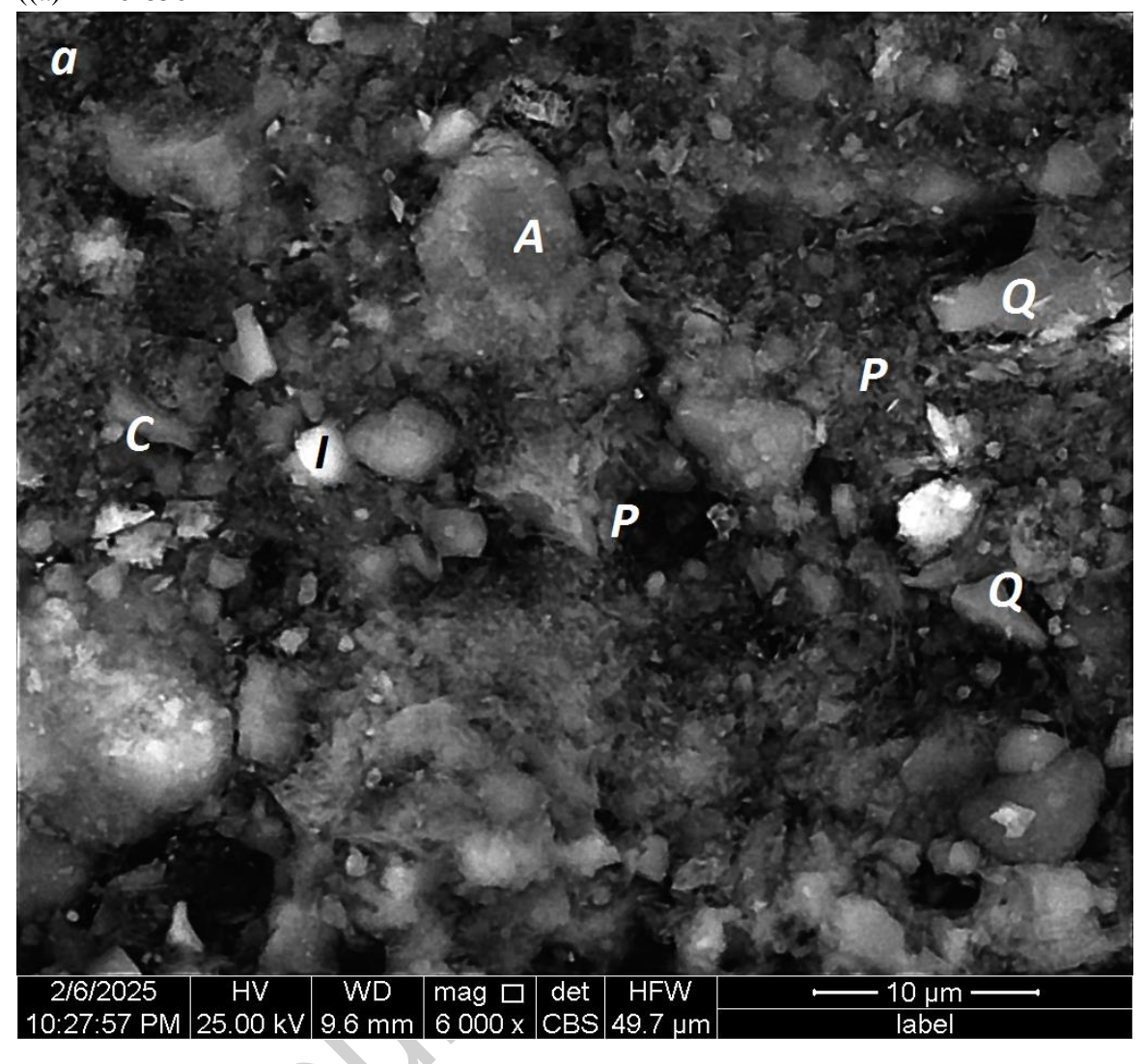
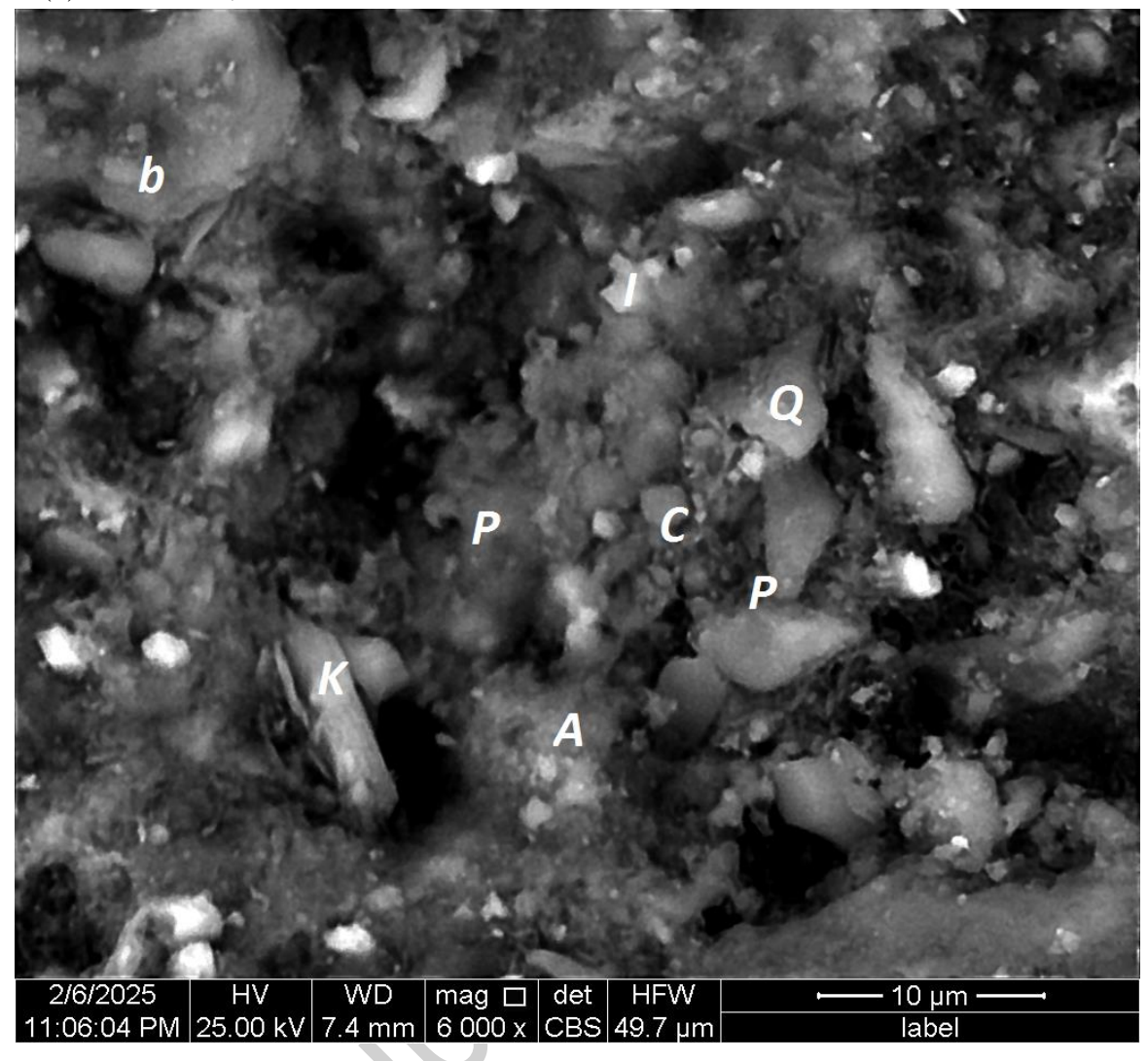


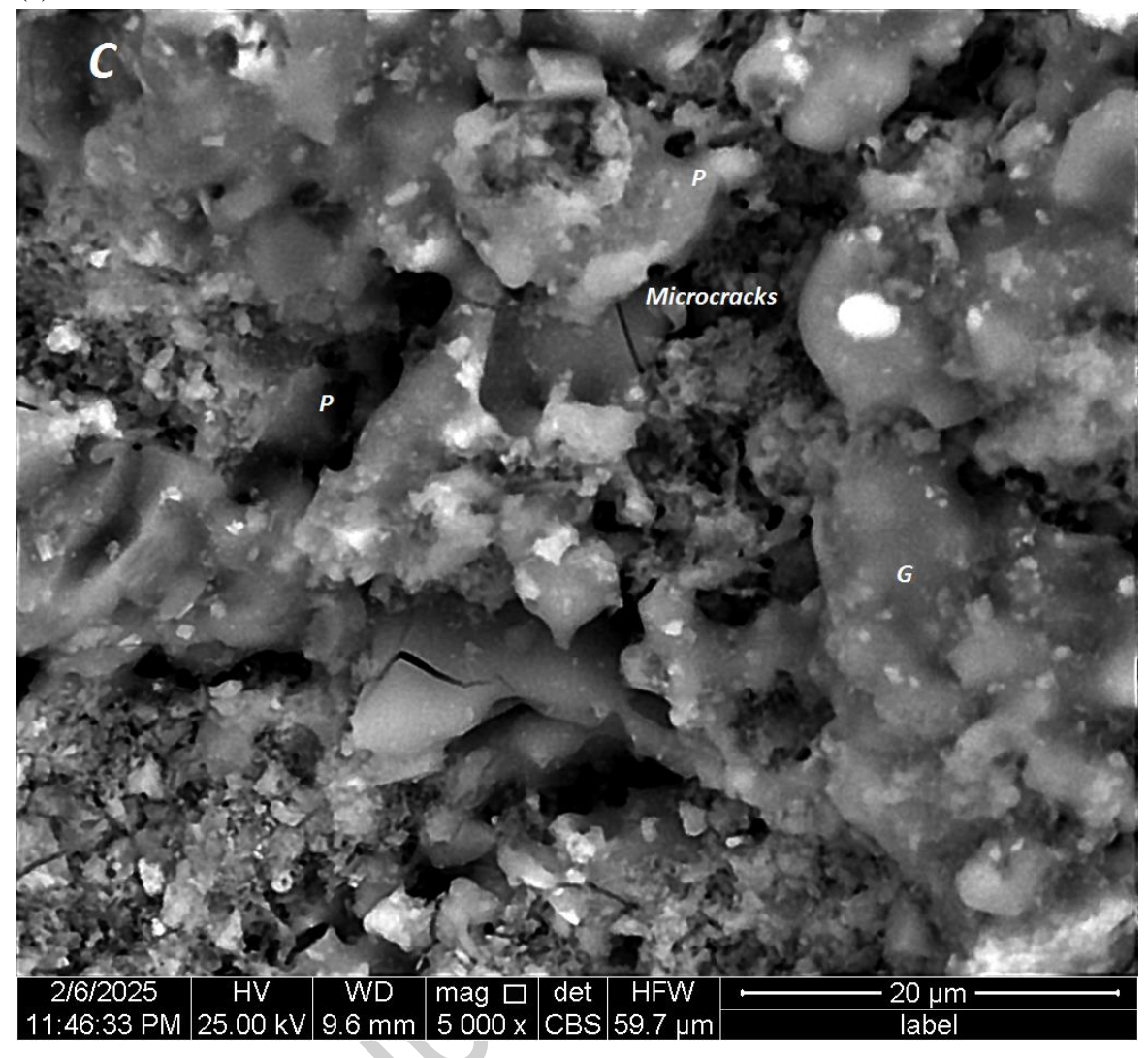
Figure.6: SEM images of the brick fired at 850 and 950 $^{\circ}$ C ((a) MB0-850



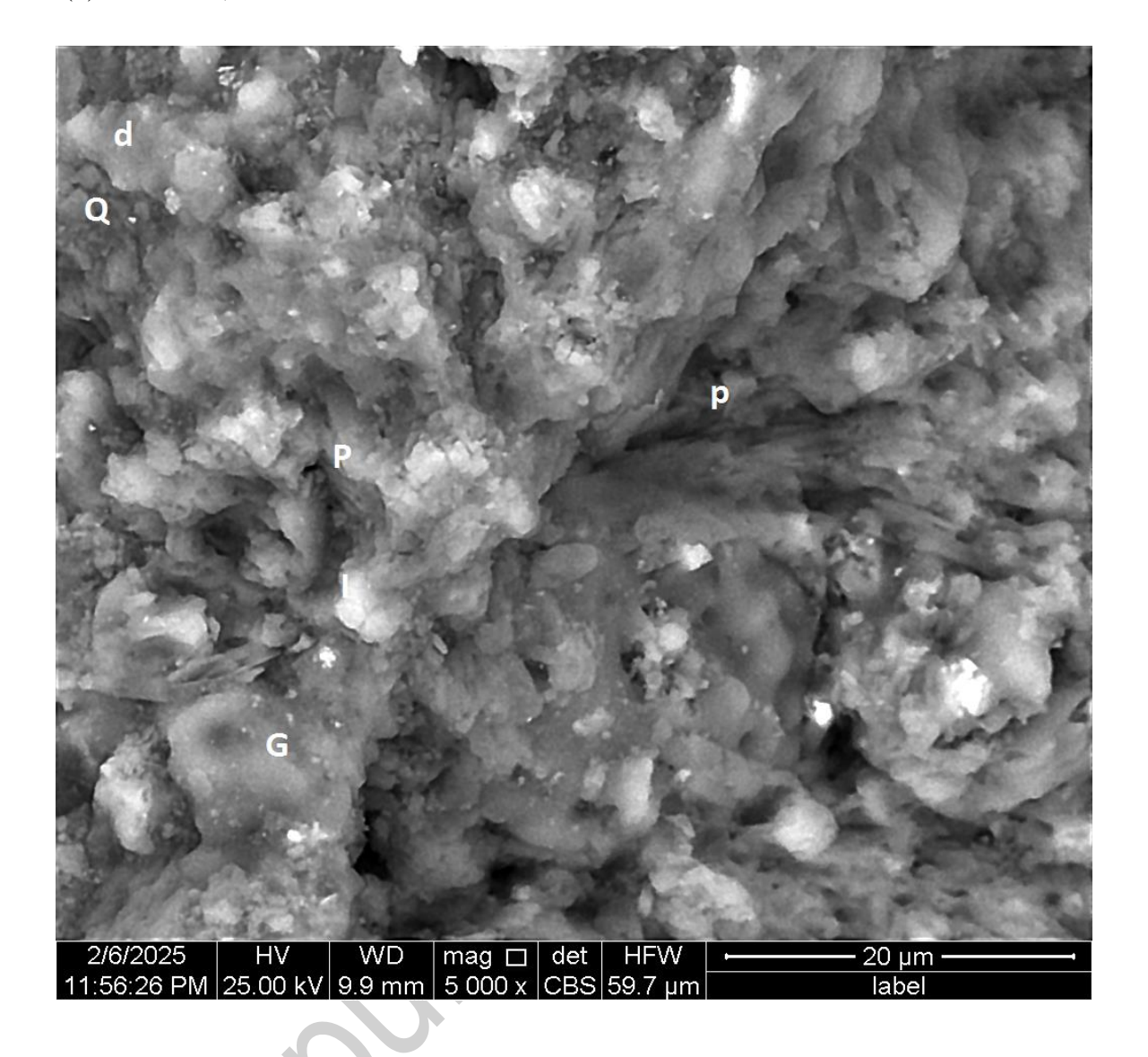
- (b) MB30- 850,



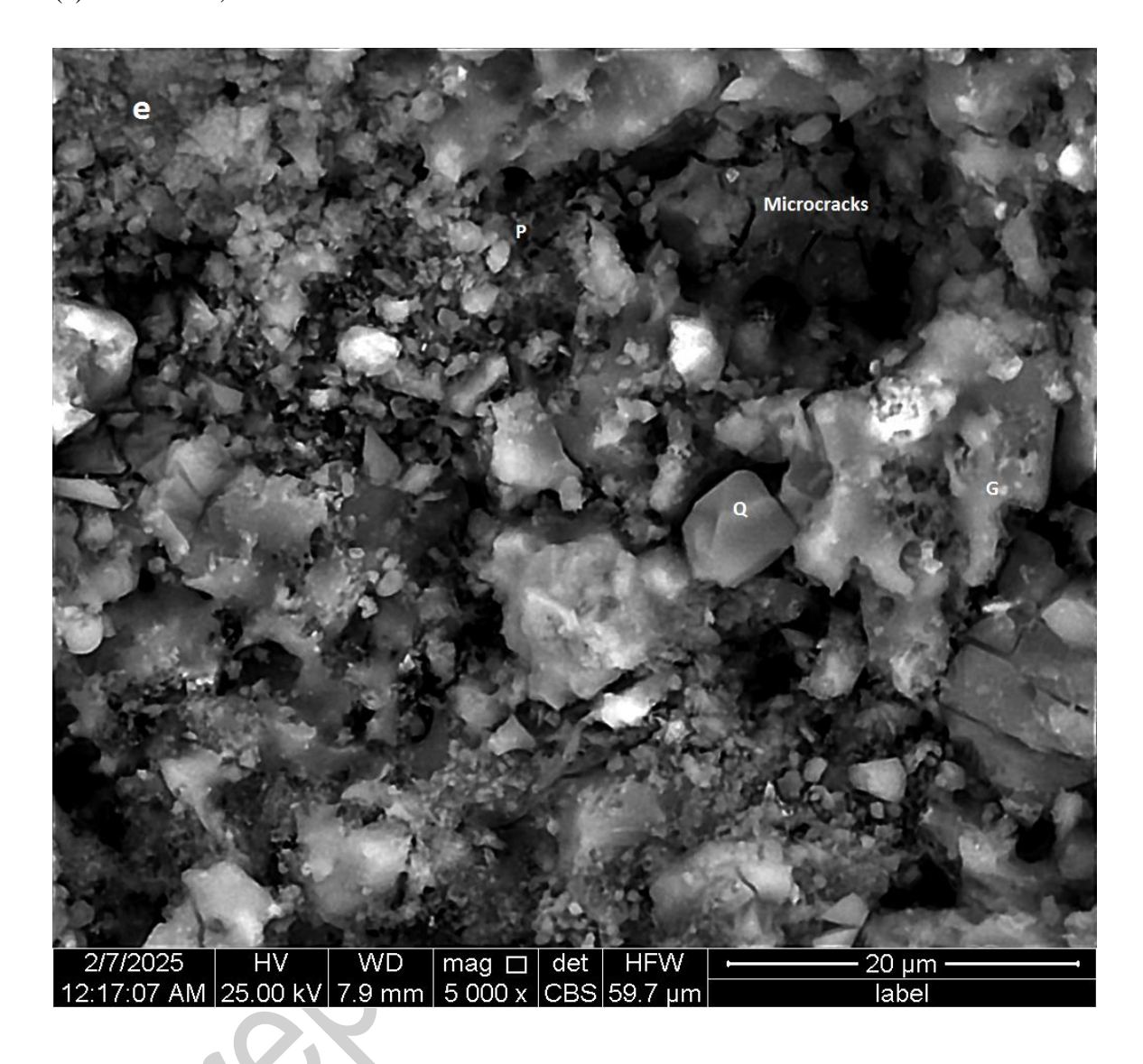
(c) MB40-850 -



(d) MB0- 950,



(e) MB30-950,



(f) MB40-950) (P: pore, I: Iron, A: agglomerates; Q: quartz, C: Calcite, G: glass, K: kaolinite).

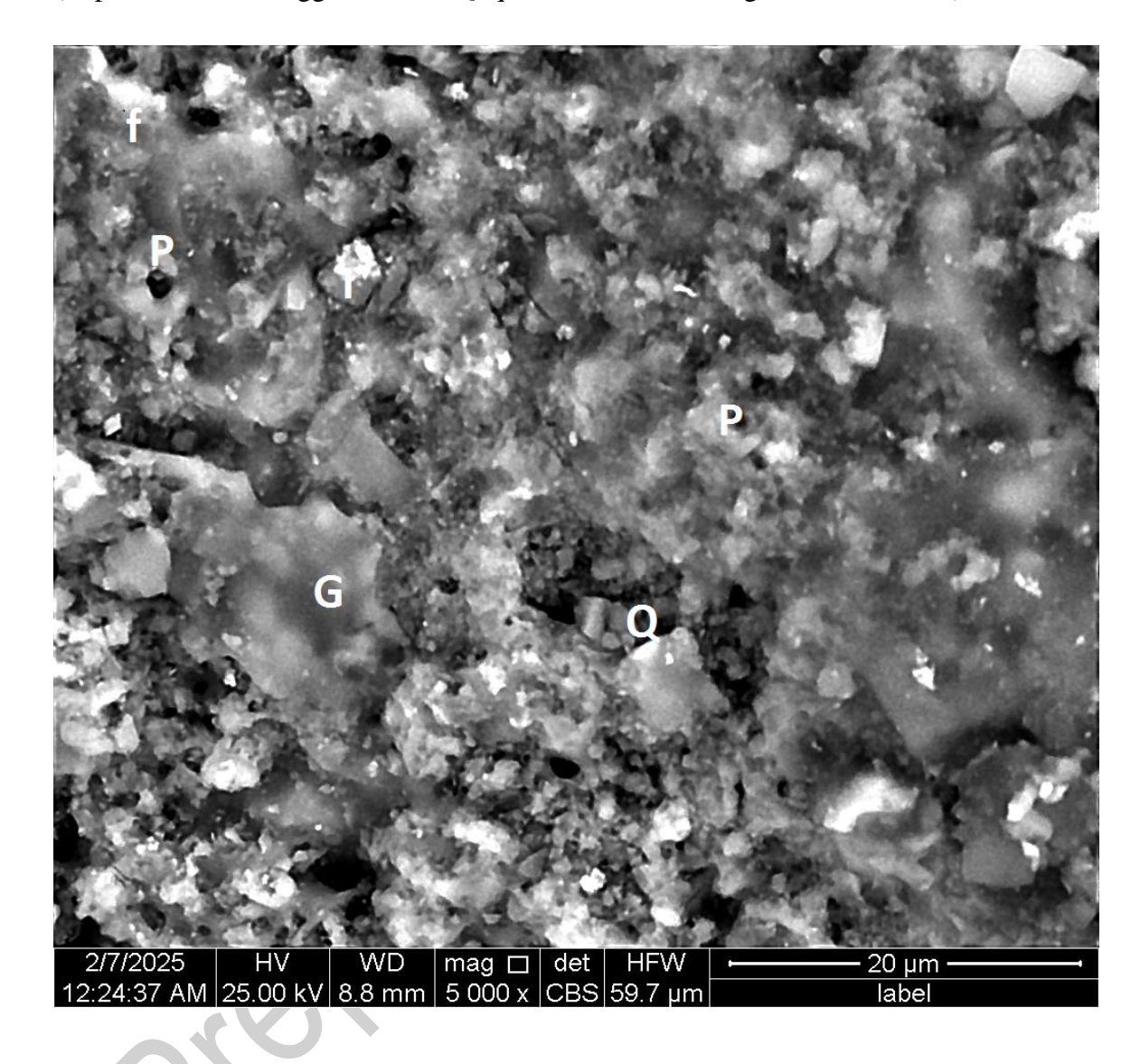


Figure.7: Compressive strength of the bricks as a function of IMW additions.

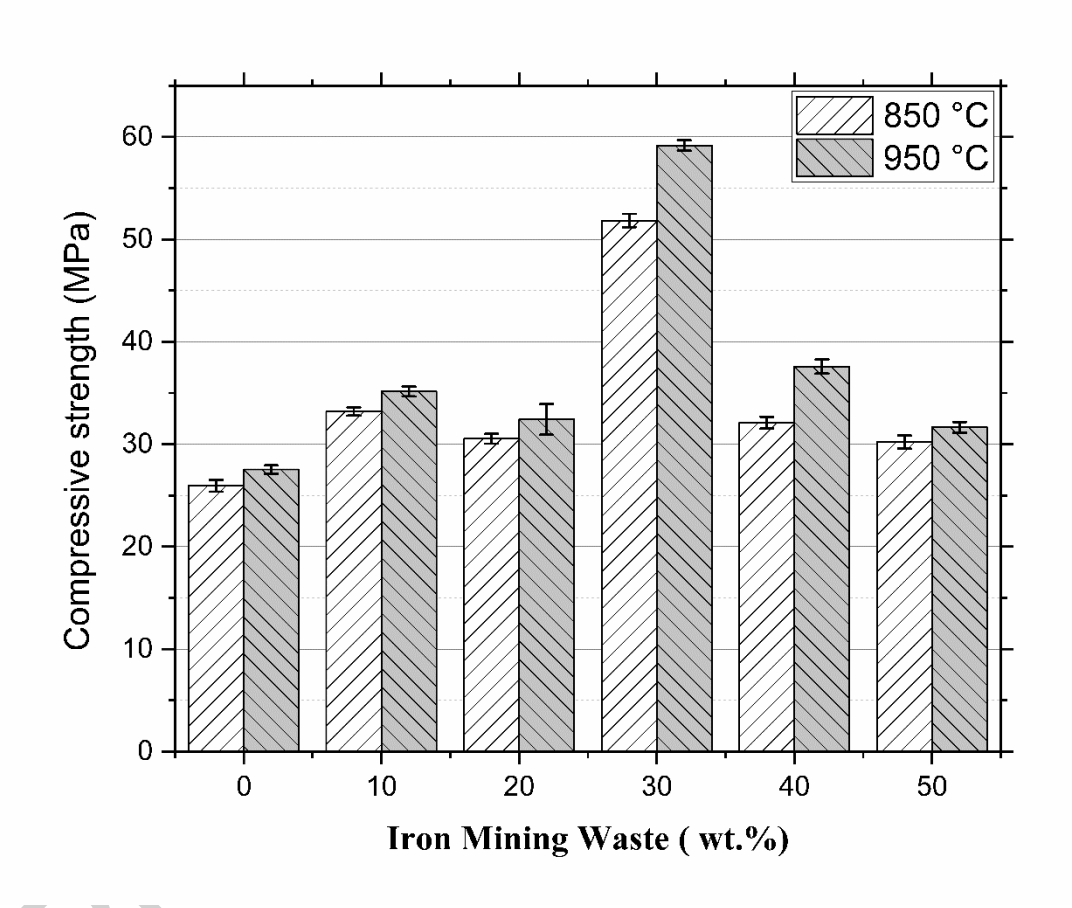


Figure.8: Flexural strength of the bricks as function of IMW additions.

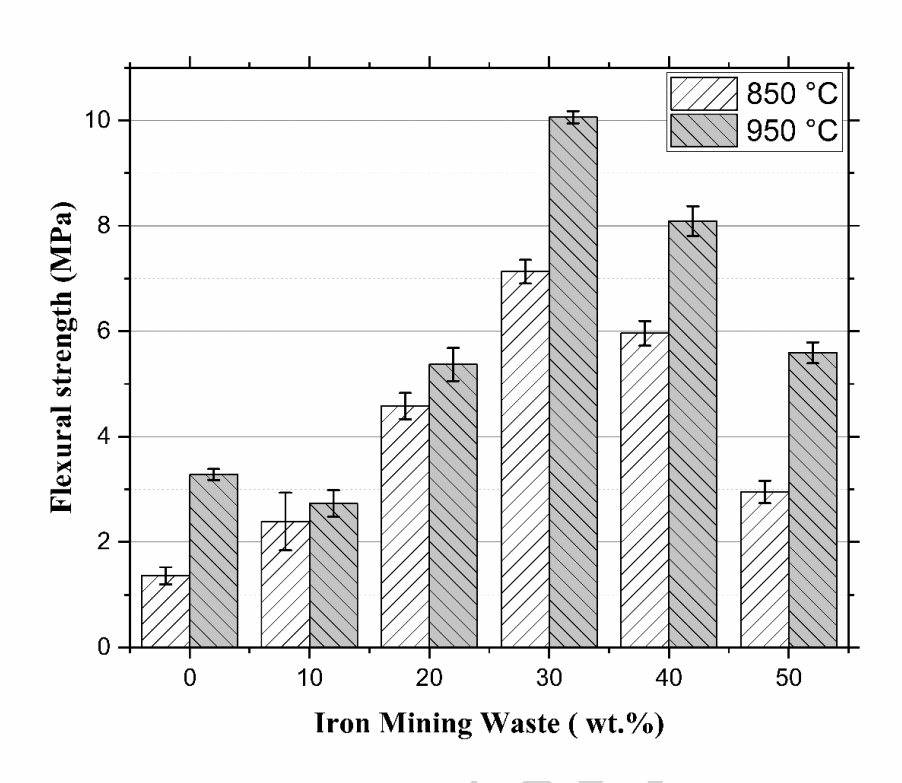


Figure.9: Thermal conductivity of the bricks as function of IMW additions.

